Supplementary information for

A thermodynamic framework for bulk–surface partitioning in finite-volume mixed organic–inorganic aerosol particles and cloud droplets

Ryan Schmedding[1] and Andreas Zuend[1]

[1]Department of Atmospheric and Oceanic Sciences, McGill University, Montreal, Quebec, Canada

Correspondence: Andreas Zuend (andreas.zuend@mcgill.ca)
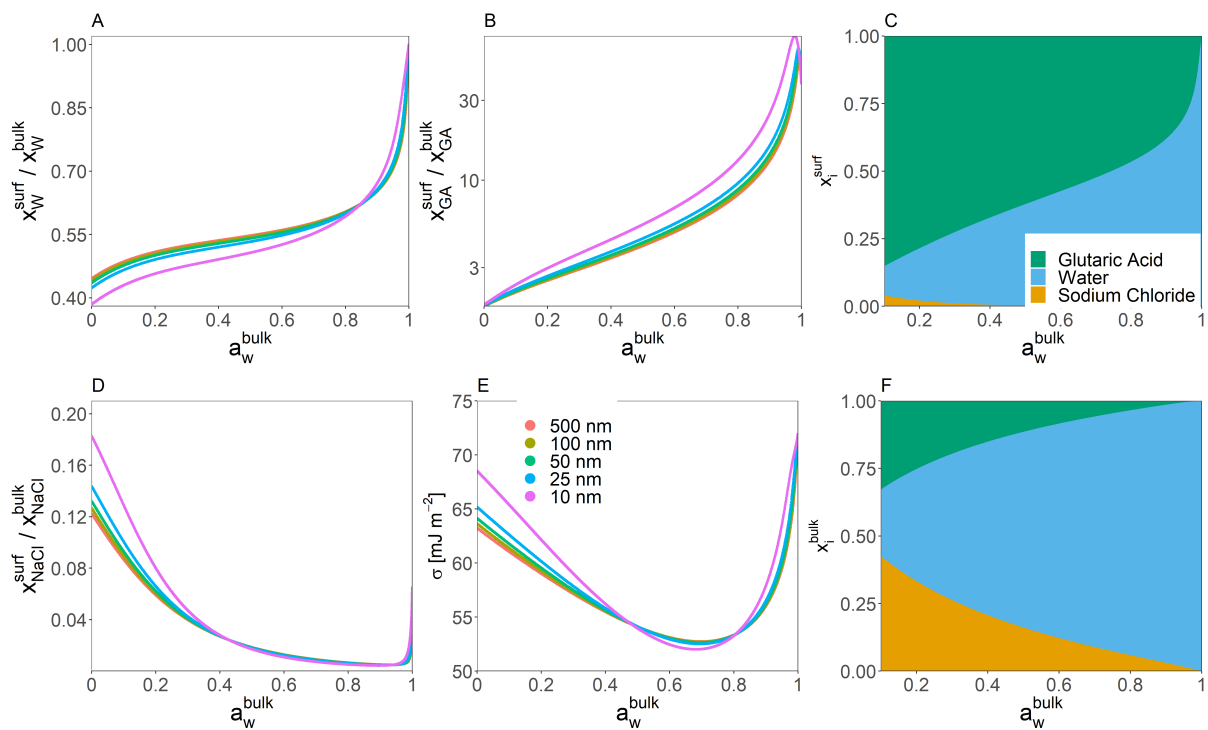
Figure S1. Predicted bulk–surface partitioning coefficient ($\frac{x_i^{\mathrm{surf}}}{x_i^{\mathrm{bulk}}}$) of (A) water, (B) glutaric acid, and (D) sodium chloride present in a forced single-bulk-phase particle at $T = 298$ K as a function of a_w^{bulk}. Right column (composition bar graphs): shown are the mole fractions of each species in the surface and the bulk phase (α) for the particle of 25 nm dry diameter.
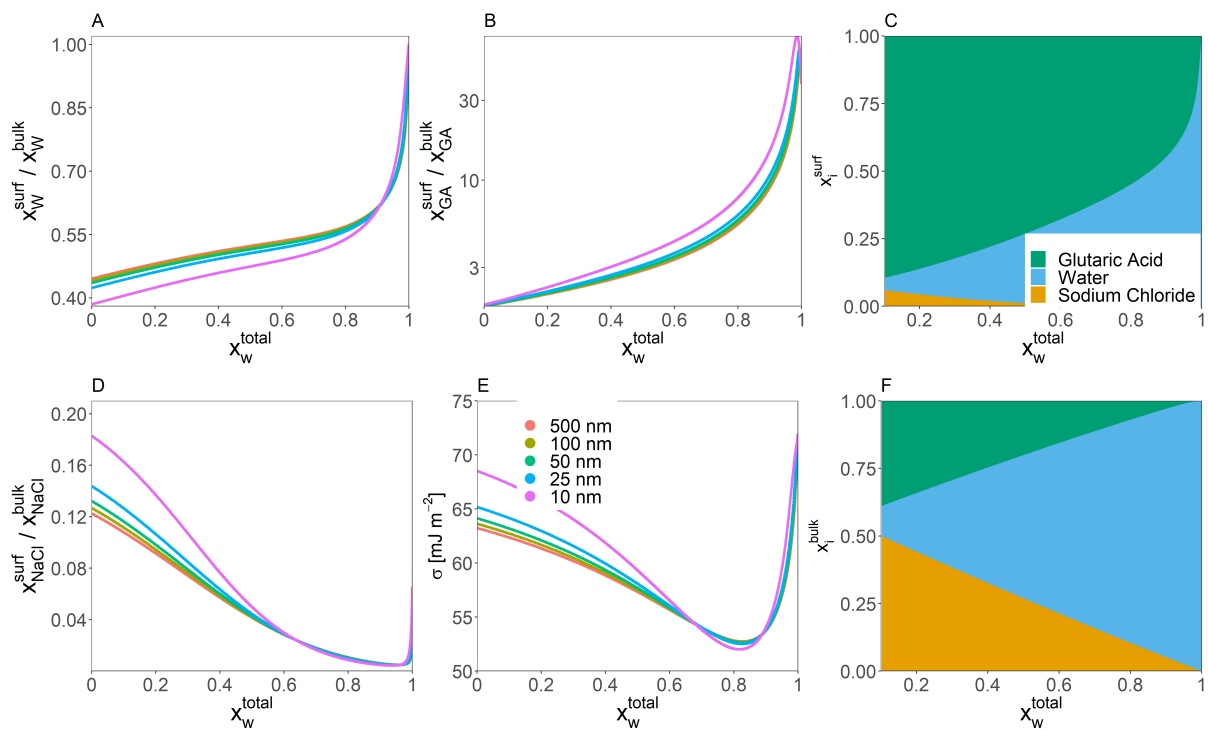
Figure S2. Predicted bulk–surface partitioning coefficient ($\frac{x_i^{\text{surf}}}{x_i^{\text{bulk}}}$) of (A) water, (B) glutaric acid, and (D) sodium chloride present in a forced single-bulk-phase particle at $T = 298$ K as a function of x_w^{total}. Right column (composition bar graphs): shown are the mole fractions of each species in the surface and the bulk phase (α) for the particle of 25 nm dry diameter.
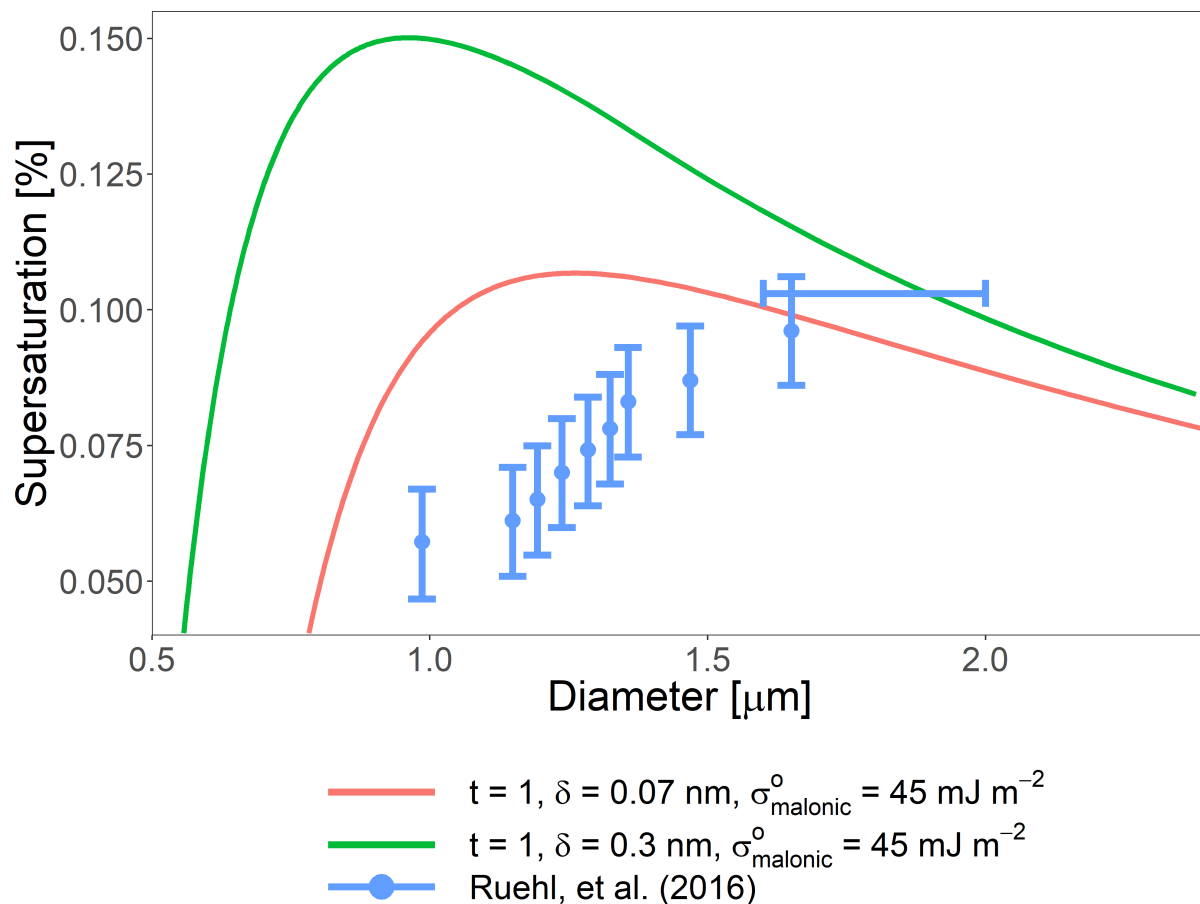
Figure S3. Predicted saturation ratio for a ternary water–malonic-acid–ammonium-sulfate system corresponding to a 50 nm diameter ammonium sulfate core coated to a total diameter of 150 nm with malonic acid, corresponding to measurements by Ruehl et al. (2016). In order to better match the experimental data better, δ was set to 0.07 nm. No combination of t and modifications to $\sigma^\circ_{\text{malonic}}$ were able to capture both the points leading up to the critical supersaturation and the critical supersaturation itself. Also shown is a prediction using the more standard assumptions that $t = 1$, $\delta = 0.3$ nm, and $\sigma^\circ_{\text{malonic}} = 45.0 \, \text{mJ m}^{-2}$ (Hyvärinen et al., 2006) The horizontal bar represents the critical supersaturation for cloud activation Ruehl et al. (2016).
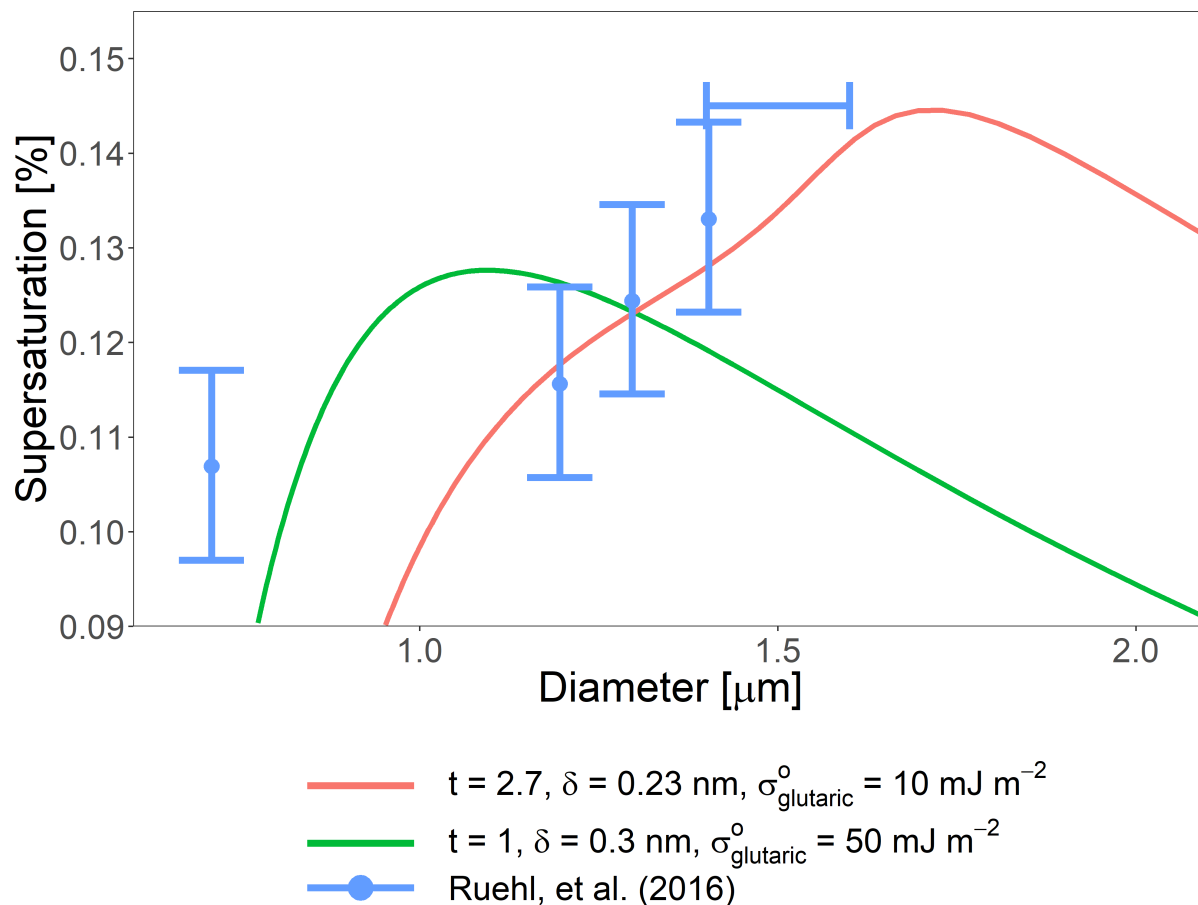
Figure S4. Predicted saturation ratio for a ternary water–glutaric-acid–ammonium-sulfate system corresponding to a 50 nm diameter ammonium sulfate core coated to a total diameter of 150 nm with glutaric acid, corresponding to measurements by Ruehl et al. (2016). In order to better match the experimental data better, δ was set to 0.23 nm. t was set to 2.7 and $\sigma^{\circ}_{\text{glutaric}}$ was set to 10 mJ m^{-2}. Also shown is a prediction using the more standard assumptions that $t = 1$, $\delta = 0.3$ nm, and $\sigma_{\text{glutaric}} = 50$ mJ m^{-2} (Ruehl et al., 2016; Hyvärinen et al., 2006; Booth et al., 2009) The horizontal bar represents the critical supersaturation for cloud activation Ruehl et al. (2016).
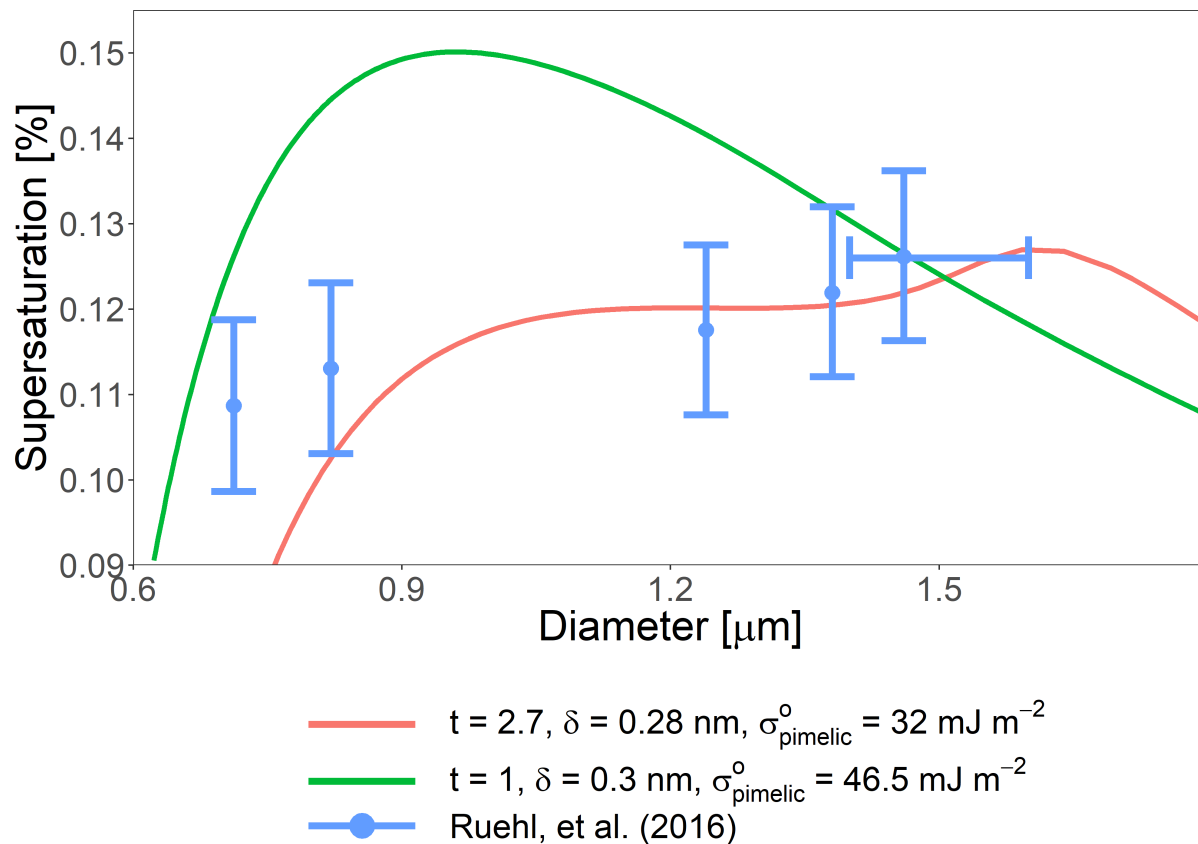
Figure S5. Predicted saturation ratio for a ternary water–pimelic-acid–ammonium-sulfate system corresponding to a 50 nm diameter ammonium sulfate core coated to a total diameter of 150 nm with succinic acid, corresponding to measurements by Ruehl et al. (2016). In order to better match the experimental data better, δ was set to 0.28 nm, t was set to 2.7 and σ_{pimelic} was set to 32 mJ m^{-2} Also shown is a prediction using the more standard assumptions that $t = 1$, $\delta = 0.3$ nm, and $\sigma_{\text{pimelic}} = 46.5$ mJ m^{-2} based on similartiy to other surface tensions of similar dicarboxylic acids reported by Hyvärinen et al. (2006). The horizontal bar represents the critical supersaturation for cloud activationRuehl et al. (2016).
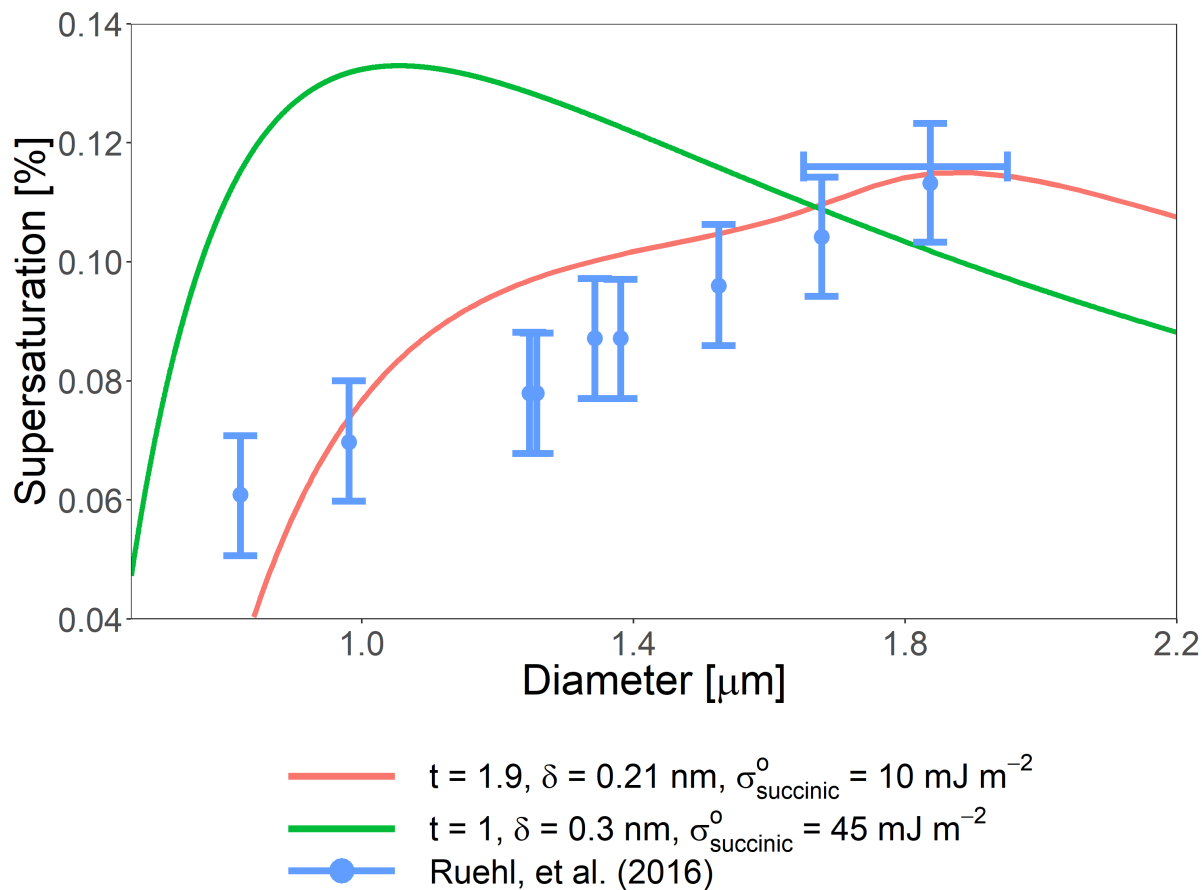
Figure S6. Predicted saturation ratio for a ternary water–succinic-acid–ammonium-sulfate system corresponding to a 50 nm diameter ammonium sulfate core coated to a total diameter of 150 nm with succinic acid, corresponding to measurements by Ruehl et al. (2016). In order to better match the experimental data better, $\sigma^{\circ}_{\mathrm{succinic}}$ was set to $10\,\mathrm{mJ\,m^{-2}}$, δ was set to 0.21 nm, the value of t was set to 1.9. Also shown is a prediction using the more standard assumptions that $t = 1$, $\delta = 0.3$ nm, and $\sigma^{\circ}_{\mathrm{succinic}} = 45.0\,\mathrm{mJ\,m^{-2}}$ (Hyvärinen et al., 2006) The horizontal bar represents the critical supersaturation for cloud activation Ruehl et al. (2016).
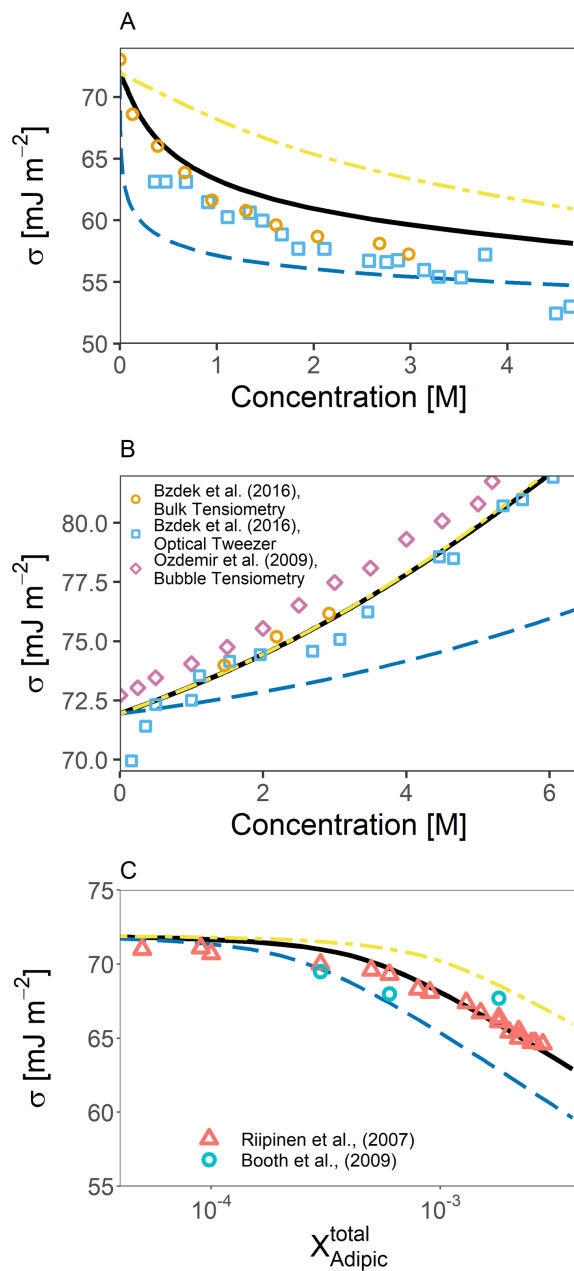
Figure S7. Predicted solution surface tensions assuming a 10% reduction or increase in σ°_{solute} (blue and yellow curves respectively) for the systems shown in (A) Figure 1A, (B) Figure 1B, and (C) Figure 3. All systems had a starting particle size of 5 μm and $\delta = 0.3$ nm

Table S1. Surrogate component concentrations for isoprene-derived SOA based on a simulation by the Master Chemical Mechanism (Jenkin et al., 1997, 2012, 2015). The listed concentrations are total amounts (gas plus particle phase) per unit volume of air for the co-condensation scenario, as well as condensed phase concentrations only for the calculations without co-condensation of organic species. For more details, see the supplementary material of Rastak et al. (2017) and Gervasi et al. (2020).

Name (MCM)	M [g mol^{-1}]	Input Concentration [mol m^{-3}] Co-condensation Enabled	Co-condensation Disabled
IEB1OOH	150.11	3.76459×10^{-8}	2.38011×10^{-8}
IEB2OOH	150.11	6.75043×10^{-9}	1.83810×10^{-9}
C59OOH	150.09	3.92509×10^{-8}	3.11576×10^{-8}
IEC1OOH	150.09	1.37006×10^{-8}	1.08756×10^{-8}
C58OOH	150.11	3.91125×10^{-9}	2.47284×10^{-9}
IEPOXA	118.13	2.56541×10^{-15}	8.11516×10^{-19}
C57OOH	150.11	3.17789×10^{-9}	2.00918×10^{-9}
IEPOXC	118.13	1.99219×10^{-14}	2.61410×10^{-17}
HIEB1OOH	166.11	1.92764×10^{-9}	1.92561×10^{-9}
INDOOH	197.14	1.41401×10^{-9}	1.40886×10^{-9}
IEACO3H	148.10	1.08728×10^{-13}	4.00883×10^{-16}
C525OOH	166.09	1.44713×10^{-9}	1.44655×10^{-9}
HIEB2OOH	166.11	9.55507×10^{-10}	9.48692×10^{-10}
IEC2OOH	148.06	7.53565×10^{-13}	1.56989×10^{-14}
INAOOH	197.14	7.93083×10^{-10}	7.82336×10^{-10}
C510OOH	195.10	7.27167×10^{-11}	2.37637×10^{-11}
INB1OOH	197.14	4.04138×10^{-10}	4.02731×10^{-10}
IECCO3H	148.11	4.87375×10^{-13}	5.69206×10^{-15}
INCOOH	197.14	1.82889×10^{-10}	1.72834×10^{-10}
INB2OOH	197.14	1.98863×10^{-10}	1.96461×10^{-10}
Tetrol Dimer	254.28	3.15073×10^{-8}	3.15073×10^{-8}

Table S2. List of abbreviations used in this work and their meanings.

Abbreviation	Meaning
VOC	Volatile Organic Compound
SVOC	Semi-Volatile Organic Compound
IVOC	Intermediate Volatility Organic Compound
LVOC	Low Volatility Organic Compound
POA	Primary Organic Aerosol
SOA	Secondary Organic Aerosol
LLPS	Liquid–Liquid Phase Separation
CCN	Cloud Condensation Nucleus
RH	Relative Humidity
LLE	Liquid–Liquid Equilibrium
AIOMFAC	Aerosol Inorganic–Organic Mixtures Functional groups Activity Coefficients
PM	Particulate matter

Table S3: List of mathematical symbols used in this work and their meanings.

Category	Symbol	Meaning	Units
Mathematical Variables	A	area of the surface	m^2
	$\mathscr{A}_i$	partial molar area of i	$\mathrm{m}^2\,\mathrm{mol}^{-1}$
	a_i	chemical activity (mole-fraction- or molality-based) of i	$-$
	A^{SL}	Szyszkowski–Langmuir fit parameter	$\mathrm{J\,m}^{-2}$
	B^{SL}	Szyszkowski–Langmuir fit parameters	$\mathrm{mol\,m}^{-3}$
	C^{SL}	bulk concentration in Szyszkowski–Langmuir model	concentration
	$A_{\circ}^{CF}$	maximum surface adsorbtion in the compressed film model	$\mathrm{mol\,m}^{-2}$
	A^{CF}	current surface adsorption in compressed film model	$\mathrm{mol\,m}^{-2}$
	D	diameter	m
	G	Gibbs energy	J
	f_i	volume fraction of i	$-$
	M_i	molar mass of i	$\mathrm{kg\,mol}^{-1}$
	n_i	number of moles	mol
	P	pressure	Pa
	R	universal gas constant	$\mathrm{J\,mol}^{-1}\,\mathrm{K}^{-1}$
	S	entropy or saturation ratio (depending on context)	$\mathrm{J\,K}^{-1}$ or $-$
	SS	supersaturation	$\%$
	T	temperature	K
	t	exponential scaling factor for surface activity coefficients	$-$
	U	internal energy	J
	V	system volume	m^3
	$\mathscr{V}_i$	molar volume of i	$\mathrm{m}^3\,\mathrm{mol}^{-1}$
	x_i	mole fraction of i	$-$
Greek Letter Variables	Γ	Gibbs surface excess	$\mathrm{mol\,m}^{-2}$
	γ_i	activity coefficient of i	$-$
	δ	thickness of Guggenheim surface phase	m
	ϵ	machine precision	$-$
	ε_i	fraction of the total particle amount of species i partitioned to the surface phase (surface fraction)	$-$
	ζ_i	fraction of i in between the maximum and minimum possible volumes it can occupy in the surface	$-$

	κ	hygroscopicity parameter	—
	μ_i	chemical potential of i	$\mathrm{J\,mol^{-1}}$
	ξ_i	intrinsic chemical potential of the surface phase of i	$\mathrm{J\,mol^{-2}}$
	ρ_i	density of i	$\mathrm{kg\,m^{-3}}$
	σ_i	surface tension of i	$\mathrm{J\,m^{-2}}$
	b	bulk phase	—
	c	thermodynamic critical point	—
	CF	compressed film model	—
	$calc$	calculated value	—
	$crit$	CCN critical activation property	—
	dry	particle under dry conditions (water-free condensed phase, RH < 1 %)	—
	$guess$	initial guess	—
Superscripts	i	chemical component or species index	—
and	max	maximum	—
Subscripts	min	minimum	—
	np	non-partitioning case	—
	pm	particle phase	—
	SL	Szyszkowski–Langmuir	—
	s	surface phase	—
	rg	range	—
	tot	total	—
	w	water	—
	wet	particle under wet conditions (water present in condensed phase, RH > 1 %)	—
	α	inorganics-rich phase	—
	β	organics-rich phase	—
	ϕ	phase index	—
	$\star$	unnormalized	—
	$\circ$	standard or reference state	—

References

Booth, A. M., Topping, D. O., McFiggans, G., and Percival, C. J.: Surface tension of mixed inorganic and dicarboxylic acid aqueous solutions at 298.15 K and their importance for cloud activation predictions, Phys. Chem. Chem. Phys., 11, 8021–8028, https://doi.org/10.1039/B906849J, 2009.

Gervasi, N. R., Topping, D. O., and Zuend, A.: A predictive group-contribution model for the viscosity of aqueous organic aerosol, Atmospheric Chemistry and Physics, 20, 2987–3008, https://doi.org/10.5194/acp-20-2987-2020, 2020.

Hyvärinen, A.-P., Lihavainen, H., Gaman, A., Vairila, L., Ojala, H., Kulmala, M., and Viisanen, Y.: Surface Tensions and Densities of Oxalic, Malonic, Succinic, Maleic, Malic, and cis-Pinonic Acids, Journal of Chemical & Engineering Data, 51, 255–260, https://doi.org/10.1021/je050366x, 2006.

Jenkin, M. E., Saunders, S. M., and Pilling, M. J.: The tropospheric degradation of volatile organic compounds: a protocol for mechanism development, Atmospheric Environment, 31, 81–104, https://doi.org/https://doi.org/10.1016/S1352-2310(96)00105-7, 1997.

Jenkin, M. E., Wyche, K. P., Evans, C. J., Carr, T., Monks, P. S., Alfarra, M. R., Barley, M. H., McFiggans, G. B., Young, J. C., and Rickard, A. R.: Development and chamber evaluation of the MCM v3.2 degradation scheme for β-caryophyllene, Atmospheric Chemistry and Physics, 12, 5275–5308, https://doi.org/10.5194/acp-12-5275-2012, 2012.

Jenkin, M. E., Young, J. C., and Rickard, A. R.: The MCM v3.3.1 degradation scheme for isoprene, Atmospheric Chemistry and Physics, 15, 11 433–11 459, https://doi.org/10.5194/acp-15-11433-2015, 2015.

Rastak, N., Pajunoja, A., Acosta Navarro, J. C., Ma, J., Song, M., Partridge, D. G., Kirkevåg, A., Leong, Y., Hu, W. W., Taylor, N. F., Lambe, A., Cerully, K., Bougiatioti, A., Liu, P., Krejci, R., Petäjä, T., Percival, C., Davidovits, P., Worsnop, D. R., Ekman, A. M. L., Nenes, A., Martin, S., Jimenez, J. L., Collins, D. R., Topping, D., Bertram, A. K., Zuend, A., Virtanen, A., and Riipinen, I.: Microphysical explanation of the RH-dependent water affinity of biogenic organic aerosol and its importance for climate, Geophysical Research Letters, 44, 5167–5177, https://doi.org/https://doi.org/10.1002/2017GL073056, 2017.

Ruehl, C. R., Davies, J. F., and Wilson, K. R.: An interfacial mechanism for cloud droplet formation on organic aerosols, Science, 351, 1447–1450, https://doi.org/10.1126/science.aad4889, 2016.